# Supplementary Information for "Formation of Intrinsic Point Defects in AlN: a study of donor and acceptor characteristics using hybrid QM/MM techniques"

**Lei Zhu [a b], Xingfan Zhang [a], Qing Hou [c d], You Lu [e], Thomas W. Keal [e], John Buckeridge [f], C. Richard A. Catlow [a g *], and Alexey A. Sokol [a *]**

[a] Department of Chemistry, University College London, London, WC1H 0AJ, United Kingdom.

[b] Department of Materials, University of Oxford, Parks Road, Oxford OX1 3PH, UK.

[c] School of Artificial Intelligence Science and Technology, University of Shanghai for Science and Technology, Shanghai, 200093, China

[d] Institute of Photonic Chips, University of Shanghai for Science and Technology, Shanghai, China

[e] STFC Scientific Computing, Daresbury Laboratory, Warrington, Cheshire WA4 4AD, United Kingdom

[f] School of Engineering, London South Bank University, London, SE1 6NG, United Kingdom

[g] School of Chemistry, Cardiff University, Park Place, Cardiff CF10 1AT, United Kingdom

* c.r.a.catlow@ucl.ac.uk; a.sokol@ucl.ac.uk

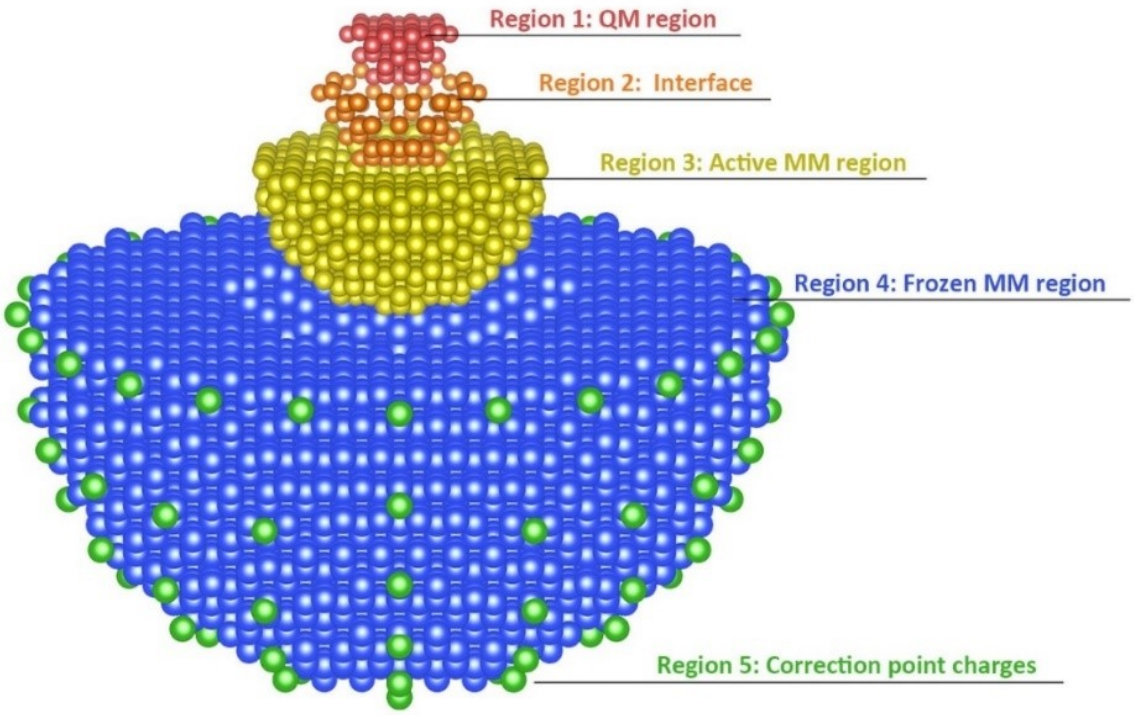


**Figure S1** The schematic diagram of embedded QM/MM cluster in Chemshell.

**Table S1** Structural data (Å) after geometry optimisation calculated by Chemshell using four different hybrid functionals (PBE0, B97-2, and BB1K), compared with other DFT results, MM results, and experimental measurements in 300K and 90K. $d$ is the bond length. (One should note that the lattice constants $a$, $c$ and internal structural parameter $u$ here are characteristics of an infinite periodic crystal, so they are only meaningful in comparison of experimental, MM and DFT PBC results. For a small cluster in our Chemshell calculation, these values are measured at the central region, so that we can make sure the cluster is not distorted against the embedded environment.)

| | **QM/MM (Chemshell)** | | | **Previous DFT**[1] | **Force field**[2] | **Experiment (300K**[3] **& 90K**[4]**)** | |
|---|---|---|---|---|---|---|---|
| Functional | **PBE0** | **B97-2** | **BB1K** | **HSE03 (33% HF)** | | | |
| $a$ | 3.148 | 3.148 | 3.148 | 3.107 | 3.112 | 3.112 | 3.115 |
| $c$ | 4.976 | 4.976 | 4.976 | 4.974 | 4.983 | 4.982 | 4.988 |
| $u$ | 0.385 | 0.385 | 0.385 | 0.382 | 0.380 | 0.382 | 0.379 |
| $c/a$ | 1.581 | 1.581 | 1.581 | 1.601 | 1.601 | 1.601 | 1.601 |
| $d_{cluster}^{central}$ | 1.915 | 1.915 | 1.915 | 1.900 | 1.894 | 1.903 | 1.893 |
| $d_{cluster}^{rim}$ | 1.906 | 1.915 | 1.906 | | | | |

**Table S2** The Jost correction energies for relaxed defect structures.

| Defect charge state | Correction Energy (eV) |
|---|---|
| **0** | 0 |
| **-1 & +1** | -0.44 |
| **-2 & +2** | -1.75 |
| **-3 & +3** | -3.93 |

**Table S3** The formation energies (eV) of $V_N^{3+}$ (when $E_F = 0$) calculated using the Chemshell QM/MM interface compared with previous DFT results. Previous calculated values reported in the literature are directly measured from their corresponding defect formation energy graphs.

| DFT functional | Formation energy |
|---|---|
| B97-2 (our work) | -8.26 |
| PBE0 (our work) | -8.28 |
| BB1K (our work) | -9.28 |
| HSE[1] | -3.02 |
| HSE[5] | -3.04 |
| HSE[6] | -3.02 |
| PBE (revised band edges)[7] | -3.85 |
| PBE (revised band edges)[8] | -4.45 |
| LDA (revised band edges)[9] | -2.49 |
| LDA[10] | -2.79 |

**Table S4** The formation energies (eV) of $V_{Al}^{0}$ calculated using the Chemshell QM/MM interface compared with previous DFT results. Previous calculated values reported in the literature are directly measured from their corresponding defect formation energy graphs.

| | XC Functional | N-rich | Al-rich |
|---|---|---|---|
| **QM/MM (Chemshell)** | **B97-2** | 6.02 | 9.32 |
| | **PBE0** | 6.24 | 9.53 |
| | **BB1K** | 6.94 | 10.24 |
| | **PBE** (GGA) | 5.93 | 9.22 |
| | **Perdew81** (LDA) | 7.56 | 10.86 |
| **Previous calculcations** | **HSE** (32-33% HF)[1,5,6,11] | 6.87, 6.98, 6.81, 6.90 | 10.02, 10.12, 10.13 |
| | **PBE** (GGA, revised band edges)[7] | 7.44 | 9.66 |
| | **PBE** (GGA, revised band gap)[8] | 7.14 | 9.21 |
| | **PBE** (GGA)[12] | 6.00 | N/A |
| | **Perdew81** (LDA)[9,13] | 8.05, 6.53 | 10.20 |

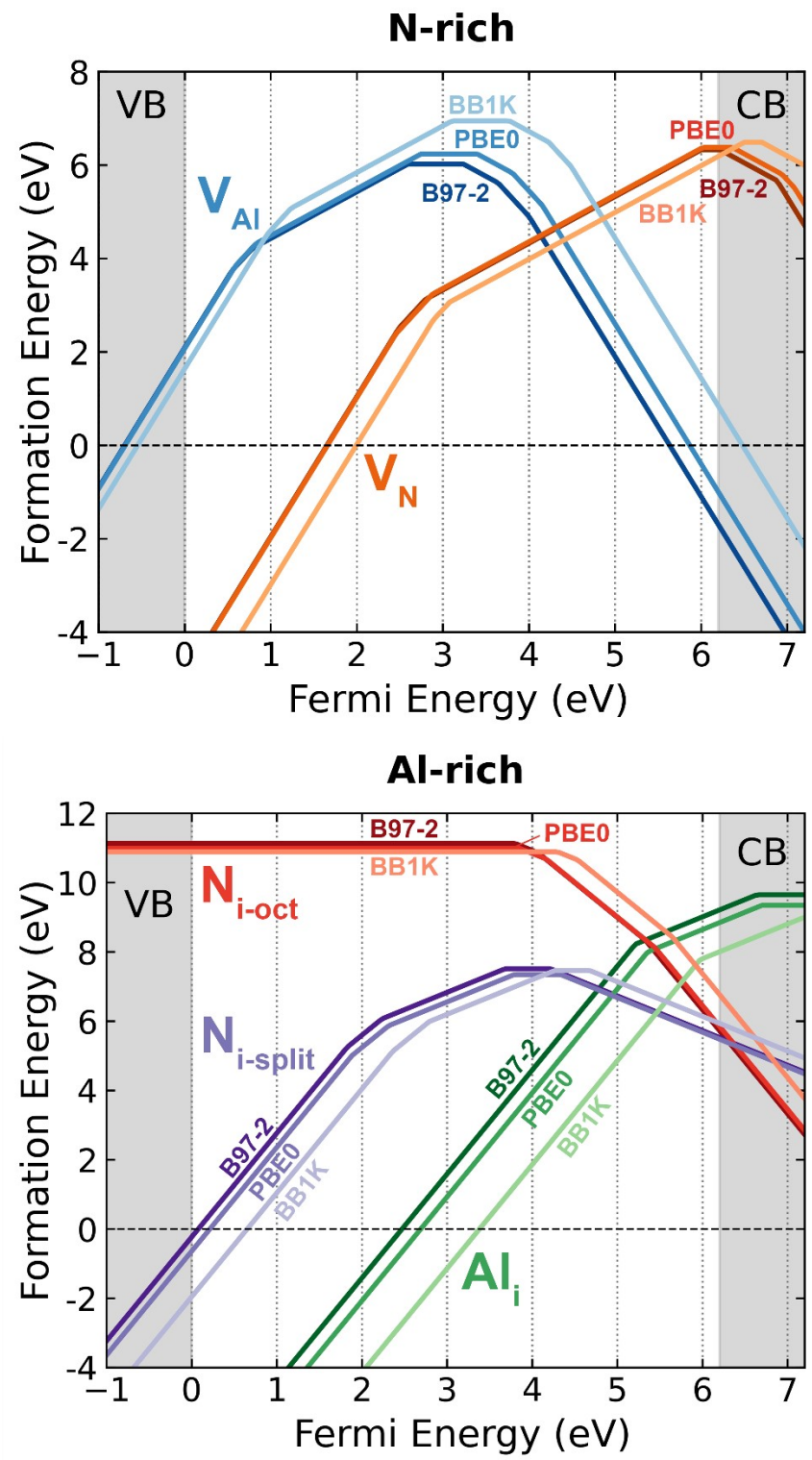


**Figure S2** Vacancy (above) and interstitial (below) defect formation energy comparison of B97-2, PBE0, BB1K functionals used in this work. Here $x = 0$ represent the VBM level. The diagrams start from 1eV below valence band (VB) maximum on the left of the x-axis and ends at 1eV above conduction band (CB) minimum on the right of the x-axis. The slopes of the lines indicate different charge states of the defect.

**Table S5** An overview of the defect energy level (eV) at the defect charge transition position with respect to the VBM. Previous calculated values reported in the literature are directly measured from their corresponding graphs. (*The HSE functional used in this report is with 25% exact HF exchange portion and screening parameter of 0.061 1/Å, unlike the rest of the HSEs with 31-33% HF exchange portion and screening parameter remained unaffected.)

| | | This work | | | Previous calculations | | | | | | |
|---|---|---|---|---|---|---|---|---|---|---|---|
| | | **B97-2** | **PBE0** | **BB1K** | **HSE**[1] | **HSE**[11] | **HSE**[5] | **HSE**[6] | **HSE**[(*)14] | **GGA**[8] | **LDA**[9] |
| $V_N$ | $(+3\|+2$ | 2.49 | 2.46 | 2.89 | 0.87 | 1.42 | 0.84 | 1.01 | | 1.52 | 0.71 |
| | $(+2\|+1$ | 2.80 | 2.88 | 3.08 | 1.08 | $(+3\|+1)$ | 1.01 | 1.17 | | $(+3\|+1)$ | $(+3\|+1)$ |
| | $(+1\|0)$ | 6.00 | 6.02 | 6.51 | 4.60 | 4.65 | 4.44 | 4.61 | | 4.22 | 5.05 |
| $V_{Al}$ | $(-2\|-3)$ | 4.00 | 4.16 | 4.49 | 3.20 | 2.85 | 3.14 | 3.09 | | 1.77 | 1.34 |
| | $(-1\|-2)$ | 3.64 | 3.81 | 4.23 | 2.96 | 2.48 | 2.88 | 2.64 | | 1.08 | 1.13 |
| | $(0\|-1)$ | 3.32 | 3.40 | 3.78 | 2.54 | 2.15 | 2.42 | 2.38 | | 0.92 | 0.83 |
| $N_{i-split}$ | $(-1\|0)$ | 4.21 | 4.33 | 4.67 | 2.82 | 2.70 | | | 3.07 | | |
| | $(0\|+1)$ | 3.68 | 3.79 | 4.27 | 2.16 | 2.12 | | | 2.69 | | |
| | $(+1\|+2$ | 2.24 | 2.32 | 2.79 | 0.94 | 1.88 | | | 0.70 | | |
| | $(+2\|+3$ | 1.83 | 1.88 | 2.36 | | 1.17 | | | | | |
| $N_{i-oct}$ | $(0\|-1)$ | 4.11 | 4.13 | 4.50 | | | | | | | |
| | $(-1\|-2)$ | 4.49 | 4.53 | 4.94 | | | | | | | |
| | $(-2\|-3)$ | 4.99 | 5.16 | 4.44 | | | | | | | |
| $Al_i$ | $(+3\|+1$ | 5.21 | 5.36 | 5.97 | 3.92 | | | | | | |
| | $(+1\|0)$ | 6.64 | 6.70 | 7.19 | 5.82 | | | | | | |
| $N_{Al,A}(-2\|-1)$ | | 4.21 | 4.26 | 4.52 | | | | | | | |
| $N_{Al,A}(-1\|0)$ | | 3.97 | 4.03 | 4.31 | 3.63 $(-2\|0)$ | 3.68 | | | | | |
| $N_{Al,B}(-1\|0)$ | | 4.05 | 4.35 | 4.79 | | | | | | | |
| $N_{Al,A}(0\|+1)$ | | 2.97 | 3.13 | 3.63 | 2.30 | | | | | | |
| $N_{Al,B}(0\|+1)$ | | 4.01 | 4.12 | 4.63 | | 2.01 $(0\|+2)$ | | | | | |
| $N_{Al,A}(+1\|+2)$ | | 2.26 | 2.38 | 2.90 | 1.99 | | | | | | |
| $N_{Al,B}(+1\|+2)$ | | 2.98 | 3.01 | 3.42 | | | | | | | |
| $N_{Al,A}(+2\|+3)$ | | 2.20 | 2.32 | 2.72 | | 0.40 | | | | | |
| $N_{Al,B}(+2\|+3)$ | | 2.55 | 2.65 | 3.01 | | | | | | | |

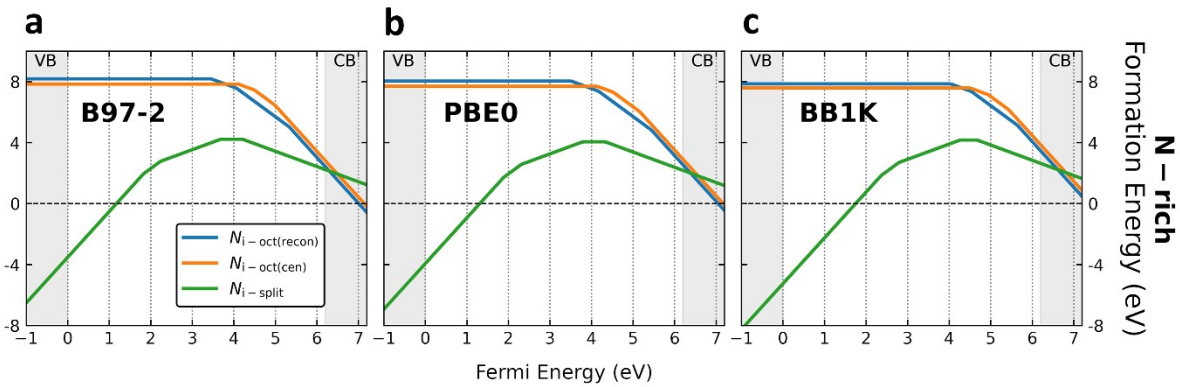


**Figure S3** The lowest defect formation energies of three N interstitial types with respect to Fermi level energies are calculated using B97-2, PBE0, and BB1K functionals.

**Note S1: Calculating diffuse state of defect**

Apart from the "compact" states of defects, in dielectrics, any charged defect can trap one or more electrons or holes in "diffuse" atom-like states of large effective radius. Such states of a charged defects can be modelled computationally using the effective mass theory[15], where an electron (or a hole) can be effectively represented by an atomic (e.g., hydrogenic) state centred on the compact charged defect. In the context of current defect calculations using the QM/MM embedded cluster approach, this approach was first realised by Buckeridge et al[16]. The "attaching energies", a term describing electrons and holes attached to compact defects in different charge states, can be calculated using the formulae below:

$$E_H = -\frac{m^*}{2\varepsilon^2}Z^2 \qquad \text{for } 1e \text{ or } 1h \text{ (Hydrogen type)},$$

$$E_{Hydride} = \frac{m^*}{\varepsilon^2}(I_H - A_H) \qquad \text{for } 2e \text{ or } 2h \text{ (Hydride type)},$$

$$E_{He} = \frac{m^*}{\varepsilon^2}I_{He}^{2nd} \qquad \text{for } 1e \text{ or } 1h \text{ (Helium type)},$$

$$E_{He} = \frac{m^*}{\varepsilon^2}(I_{He}^{1st} + I_{He}^{2nd}) \qquad \text{for } 2e \text{ or } 2h \text{ (Helium type)},$$

$$E_{Li,\,2} = \frac{m^*}{\varepsilon^2}I_{Li}^{3rd} \qquad \text{for } 1e \text{ or } 1h \text{ (Lithium type)},$$

$$E_{Li,\,2} = \frac{m^*}{\varepsilon^2}(I_{Li}^{2nd} + I_{Li}^{3rd}) \qquad \text{for } 2e \text{ or } 2h \text{ (Lithium type)},$$

$$E_{Li,\,3} = \frac{m^*}{\varepsilon^2}(I_{Li}^{1st} + I_{Li}^{2nd} + I_{Li}^{3rd}) \qquad \text{for } 3e \text{ or } 3h \text{ (Lithium type)},$$

where $E_H$, $E_{He}$, $E_{Li}$, and $E_{Hydride}$ are the attaching energies of diffuse states, $m^*$ is the respective effective mass of the electron or the hole, $\varepsilon$ is dielectric constant (10.98 for adiabatic processes from our previous work[2]), $Z$ is the charge of the compact defect state, $I$ represents the ionisation potential, and $A$ represents the electron affinity ($I$ and $A$ values are summarized in Table S2). Carriers are trapped by a representative Helium atom if the compact defect charge state is +2/-2, and by a Lithium atom if the compact charge state is +3/-3. Due to the lack of experimental values of effective masses of electrons and holes in AlN, we take the theoretical values from the previous literature, which are $0.30m_0$ for the electron[3] and $0.73m_0$ for the hole[17]. All the carrier attaching energies are summarized in Tables S3 & S4.

**Table S6** A summary of the experimental ionization potentials ($I$) and electron affinities ($A$) of Helium and Lithium[18] used for calculating diffuse electrons/hole binding energies.

| | **Energy (eV)** |
|---|---|
| $I_H$ | -13.59844 |
| $A_H$ | 0.754195 |
| $I_{He}^{1st} =- A_{He}^{1st}$ | -54.41776 |
| $I_{He}^{2nd} =- A_{He}^{2nd}$ | -24.58738 |
| $I_{Li}^{1st} =- A_{Li}^{1st}$ | -122.45435 |
| $I_{Li}^{2nd} =- A_{Li}^{2nd}$ | -75.64009 |
| $I_{Li}^{3rd} - A_{Li}^{3rd}$ | -5.391719 |

**Table S7** The attaching energies (eV) of the diffuse electrons in AlN with respect.

| **Electron type** | **Defect charge, $Z$** | **Attaching energy (eV)** |
|---|---|---|
| $1e$ (Hydrogen type) | +1 | -0.034 |
| $2e$ (Hydride type) | +1 | -0.036 |
| $1e$ (Helium type) | +2 | -0.116 |
| $2e$ (Helium type) | +2 | -0.197 |
| $1e$ (Lithium type) | +3 | -0.305 |
| $2e$ (Lithium type) | +3 | -0.493 |
| $3e$ (Lithium type) | +3 | -0.506 |

**Table S8** The attaching energies (eV) of the diffuse holes in AlN with respect.

| **Hole type** | **Defect charge, $Z$** | **Attaching energy (eV)** |
|---|---|---|
| $1h$ (Hydrogen type) | -1 | -0.082 |
| $2h$ (Hydride type) | -1 | -0.087 |
| $1h$ (Helium type) | -2 | -0.328 |
| $2h$ (Helium type) | -2 | -0.476 |
| $1h$ (Lithium type) | -3 | -0.738 |
| $2h$ (Lithium type) | -3 | -1.195 |
| $3h$ (Lithium type) | -3 | -1.227 |

**Table S9** Formation energies (eV) of compact and diffuse states of $V_{Al}$ in AlN. The compact state energies are taken from the defect formation energies at VBM level. The hydrogenic state energies for diffuse electrons and holes are calculated with respect to the corresponding formation energies at VBM.

| Defect charge | Defect type | | Functional | | |
|---|---|---|---|---|---|
| | | | B97-2 | PBE0 | BB1K |
| 0 | Compact | $V_{Al}^{0}$ | 6.021 | 6.236 | 6.943 |
| | Diffuse | $V_{Al}^{1+} + 1e_{(H)}$ | 9.592 | 9.655 | 10.003 |
| | | $V_{Al}^{1-} + 1h_{(H)}$ | 9.177 | 9.553 | 10.636 |
| | | $V_{Al}^{2-} + 2h_{(He)}$ | 12.424 | 12.970 | 14.472 |
| | | $V_{Al}^{3-} + 3h_{(Li)}$ | 15.675 | 16.375 | 18.212 |
| 1- | Compact | $V_{Al}^{1-}$ | 9.259 | 9.636 | 10.718 |
| | Diffuse | $V_{Al}^{2-} + 1h_{(He)}$ | 12.572 | 13.118 | 14.620 |
| | | $V_{Al}^{3-} + 2h_{(Li)}$ | 15.708 | 16.407 | 18.245 |
| 2- | Compact | $V_{Al}^{2-}$ | 12.900 | 13.446 | 14.948 |
| | Diffuse | $V_{Al}^{3-} + 1h_{(Li)}$ | 16.164 | 16.863 | 18.701 |
| 1+ | Compact | $V_{Al}^{1+}$ | 3.426 | 3.489 | 3.837 |
| | Diffuse | $V_{Al}^{1-} + 2h_{(H)}$ | 9.172 | 9.549 | 10.632 |

**Table S10** Formation energies (eV) of compact and diffuse states of $V_N$ in AlN. The compact state energies are taken from the defect formation energies at CBM level. The hydrogenic state energies for diffuse electrons and holes are calculated with respect to the corresponding formation energies at CBM.

| Defect charge | Defect type | | Functional | | |
|---|---|---|---|---|---|
| | | | B97-2 | PBE0 | BB1K |
| 0 | Compact | $V_{N}^{0}$ | 6.326 | 6.379 | 6.490 |
| | Diffuse | $V_{N}^{1-} + 1h_{(H)}$ | 12.465 | 12.658 | 13.110 |
| | | $V_{N}^{1+} + 1e_{(H)}$ | 6.490 | 6.522 | 6.150 |
| | | $V_{N}^{2+} + 2e_{(He)}$ | 9.730 | 9.679 | 9.108 |
| | | $V_{N}^{3+} + 3e_{(Li)}$ | 13.132 | 13.110 | 12.110 |
| 1+ | Compact | $V_{N}^{1+}$ | 6.524 | 6.556 | 6.184 |
| | Diffuse | $V_{N}^{2+} + 1e_{(He)}$ | 9.792 | 9.740 | 9.169 |
| | | $V_{N}^{3+} + 2e_{(Li)}$ | 13.145 | 13.123 | 12.123 |
| 2+ | Compact | $V_{N}^{2+}$ | 9.927 | 9.876 | 9.305 |
| | Diffuse | $V_{N}^{3+} + 1e_{(Li)}$ | 13.333 | 13.312 | 12.312 |
| 1- | Compact | $V_{N}^{1-}$ | 6.347 | 6.540 | 6.992 |
| | Diffuse | $V_{N}^{1+} + 2e_{(H)}$ | 6.488 | 6.520 | 6.149 |

**Table S11** Formation energies (eV) of compact and diffuse states of $Al_i$ in AlN. The compact state energies are taken from the defect formation energies at CBM level. The hydrogenic state energies for diffuse electrons and holes are calculated with respect to the corresponding formation energies at CBM.

| Defect charge | Defect type | | Functional | | |
|---|---|---|---|---|---|
| | | | **B97-2** | **PBE0** | **BB1K** |
| 0 | Compact | $Al_i^0$ | 12.941 | 12.639 | 12.287 |
| | Diffuse | $Al_i^{1+} + 1e_{(H)}$ | 12.469 | 12.103 | 11.262 |
| | | $Al_i^{2+} + 2e_{(He)}$ | 13.498 | 12.958 | 11.654 |
| | | $Al_i^{3+} + 3e_{(Li)}$ | 13.973 | 13.313 | 11.244 |
| 1+ | Compact | $Al_i^{1+}$ | 12.503 | 12.137 | 11.296 |
| | Diffuse | $Al_i^{2+} + 1e_{(He)}$ | 13.559 | 13.019 | 11.716 |
| | | $Al_i^{3+} + 2e_{(Li)}$ | 13.986 | 13.327 | 11.257 |
| 2+ | Compact | $Al_i^{2+}$ | 13.695 | 13.154 | 11.851 |
| | Diffuse | $Al_i^{3+} + 1e_{(Li)}$ | 14.174 | 13.515 | 11.446 |

**Table S12** Formation energies (eV) of compact and diffuse states of $N_{i,oct}$. The compact state energies are taken from the defect formation energies at VBM level. The hydrogenic state energies for diffuse electrons and holes are calculated with respect to the corresponding formation energies at VBM.

| Defect charge | Defect type | | Functional | | |
|---|---|---|---|---|---|
| | | | **B97-2** | **PBE0** | **BB1K** |
| 0 | Compact | $N_{i,oct}^{0}$ | 7.833 | 7.693 | 7.586 |
| | Diffuse | $N_{i,oct}^{1-} + 1h_{(H)}$ | 11.862 | 11.744 | 12.001 |
| | | $N_{i,oct}^{2-} + 2h_{(He)}$ | 15.962 | 15.875 | 16.549 |
| | | $N_{i,oct}^{3-} + 3h_{(Li)}$ | 20.199 | 20.288 | 21.235 |
| 1- | Compact | $N_{i,oct}^{1-}$ | 11.944 | 11.826 | 12.083 |
| | Diffuse | $N_{i,oct}^{2-} + 1h_{(He)}$ | 16.110 | 16.023 | 16.697 |
| | | $N_{i,oct}^{3-} + 2h_{(Li)}$ | 20.232 | 20.320 | 21.267 |
| 2- | Compact | $N_{i,oct}^{2-}$ | 16.438 | 16.351 | 17.025 |
| | Diffuse | $N_{i,oct}^{3-} + 1h_{(Li)}$ | 20.688 | 20.777 | 21.723 |

**Table S13** Formation energies (eV) of compact and diffuse states of $N_{i,\,split}$. The compact state energies are taken from the defect formation energies at CBM level. The hydrogenic state energies for diffuse electrons and holes are calculated with respect to the corresponding formation energies at CBM.

| | | | Functional | | |
|---|---|---|---|---|---|
| **Defect charge** | **Defect type** | | **B97-2** | **PBE0** | **BB1K** |
| 0 | Compact | $N_{i,\,split}^{\;0}$ | 4.217 | 4.048 | 4.165 |
| | Diffuse | $N_{i,\,split}^{\;-1} + 1h_{(H)}$ | 8.348 | 8.299 | 8.757 |
| | | $N_{i,\,split}^{\;1+} + 1e_{(H)}$ | 6.698 | 6.422 | 6.065 |
| | | $N_{i,\,split}^{\;2+} + 2e_{(He)}$ | 10.499 | 10.144 | 9.310 |
| | | $N_{i,\,split}^{\;3+} + 3e_{(Li)}$ | 14.561 | 14.152 | 12.837 |
| 1+ | Compact | $N_{i,\,split}^{\;1+}$ | 6.732 | 6.456 | 6.098 |
| | Diffuse | $N_{i,\,split}^{\;2+} + 1e_{(He)}$ | 10.560 | 10.205 | 9.371 |
| | | $N_{i,\,split}^{\;3+} + 2e_{(Li)}$ | 14.575 | 14.165 | 12.850 |
| 2+ | Compact | $N_{i,\,split}^{\;2+}$ | 10.696 | 10.340 | 9.506 |
| | Diffuse | $N_{i,\,split}^{\;3+} + 1e_{(Li)}$ | 14.763 | 14.354 | 13.038 |
| 1- | Compact | $N_{i,\,split}^{\;1-}$ | 2.230 | 2.181 | 2.639 |
| | Diffuse | $N_{i,\,split}^{\;1+} + 2e_{(H)}$ | 6.696 | 6.420 | 6.063 |

**Table S14** Formation energies (eV) of compact and diffuse states of $N_{Al,\,A}$. The compact state energies are taken from the defect formation energies at CBM level. The hydrogenic state energies for diffuse electrons and holes are calculated with respect to the corresponding formation energies at CBM.

| | | | Functional | | |
|---|---|---|---|---|---|
| **Defect charge** | **Defect type** | | **B97-2** | **PBE0** | **BB1K** |
| 0 | Compact | $N_{Al,\,A}^{\;0}$ | 6.930 | 7.171 | 7.790 |
| | Diffuse | $N_{Al,\,A}^{\;-1} + 1h_{(H)}$ | 10.904 | 11.202 | 12.278 |
| | | $N_{Al,\,A}^{\;1+} + 1e_{(H)}$ | 10.126 | 10.203 | 10.502 |
| | | $N_{Al,\,A}^{\;2+} + 2e_{(He)}$ | 13.898 | 13.994 | 13.766 |
| | | $N_{Al,\,A}^{\;3+} + 3e_{(Li)}$ | 17.584 | 17.433 | 16.811 |
| 1+ | Compact | $N_{Al,\,A}^{\;1+}$ | 10.160 | 10.237 | 10.536 |
| | Diffuse | $N_{Al,\,A}^{\;2+} + 1e_{(He)}$ | 13.959 | 13.926 | 13.698 |
| | | $N_{Al,\,A}^{\;3+} + 2e_{(Li)}$ | 17.597 | 17.447 | 16.824 |
| 2+ | Compact | $N_{Al,\,A}^{\;2+}$ | 14.095 | 14.062 | 13.834 |
| | Diffuse | $N_{Al,\,A}^{\;3+} + 1e_{(Li)}$ | 17.785 | 17.635 | 17.012 |
| 1- | Compact | $N_{Al,\,A}^{\;1-}$ | 4.704 | 5.002 | 6.078 |
| | Diffuse | $N_{Al,\,A}^{\;1+} + 2e_{(H)}$ | 10.124 | 10.202 | 10.500 |

**Table S15** Formation energies (eV) of compact and diffuse states of $N_{Al,B}$. The compact state energies are taken from the defect formation energies at CBM level. The hydrogenic state energies for diffuse electrons and holes are calculated with respect to the corresponding formation energies at CBM.

| Defect charge | Defect type | | Functional | | |
|---|---|---|---|---|---|
| | | | **B97-2** | **PBE0** | **BB1K** |
| 0 | Compact | $N_{Al,B}^{0}$ | 7.487 | 7.481 | 8.212 |
| | Diffuse | $N_{Al,B}^{1-} + 1h_{(H)}$ | 11.540 | 11.833 | 13.005 |
| | | $N_{Al,B}^{1+} + 1e_{(H)}$ | 9.647 | 9.525 | 9.748 |
| | | $N_{Al,B}^{2+} + 2e_{(He)}$ | 12.709 | 12.556 | 12.366 |
| | | $N_{Al,B}^{3+} + 3e_{(Li)}$ | 16.049 | 15.794 | 15.247 |
| 1+ | Compact | $N_{Al,B}^{1+}$ | 9.681 | 9.558 | 9.782 |
| | Diffuse | $N_{Al,B}^{2+} + 1e_{(He)}$ | 12.770 | 12.617 | 12.427 |
| | | $N_{Al,B}^{3+} + 2e_{(Li)}$ | 16.062 | 15.807 | 15.261 |
| 2+ | Compact | $N_{Al,B}^{2+}$ | 12.906 | 12.752 | 12.562 |
| | Diffuse | $N_{Al,B}^{3+} + 1e_{(Li)}$ | 16.250 | 15.996 | 15.449 |
| 1- | Compact | $N_{Al,B}^{1-}$ | 5.340 | 5.633 | 6.805 |
| | Diffuse | $N_{Al,B}^{1+} + 2e_{(H)}$ | 9.646 | 9.523 | 9.746 |

**Note S2**:

**Computational detail of calculating density of states (DOS) using VASP**

Our ab-initio calculations were performed using a plane-wave/pseudopotential DFT approach as implemented in the Vienna Ab-initio Simulation Package (VASP)[19–21]. A 32-atom 2x2x2 wurtzite structure AlN supercell was constructed. To obtain computationally consistent results with our QM/MM simulations, the hybrid generalized gradient approximation (GGA) exchange-correlation functionals of Perdew Burke-Ernzerhof modified with a predefined amount of exact exchange (PBE0)[22,23] is used. The planewave-type basis sets with a kinetic energy cut-off of 500 eV and a gaussian smearing of 0.01 were implemented for the self-consistent field (SCF) method calculations, with a convergence criterion of $1x10^{-6}$ eV. A k-point grid of 4x4x4 was used for bulk AlN system for electronic structure calculations. The band gap value (6.11eV) was obtained with no geometry optimisation of the structure.

**Table S16** The nitrogen chemical potential calculated from the experimental thermochemical enthalpy and entropy of $N_2$. (The first column: temperature (K). The top row: $N_2$ partial pressure (atm)).

| | 1E-10 | 1E-09 | 1E-08 | 1E-07 | 1E-06 | 1E-05 | 1E-04 | 1E-03 | 1.E-02 | 1E-01 | 1E+00 | 1E+01 | 1E+02 | 1E+03 | 1E+04 | 1E+05 | 1E+06 |
|---|---|---|---|---|---|---|---|---|---|---|---|---|---|---|---|---|---|
| **300** | -0.550 | -0.520 | -0.491 | -0.461 | -0.431 | -0.401 | -0.371 | -0.342 | -0.312 | -0.282 | -0.252 | -0.223 | -0.193 | -0.163 | -0.133 | -0.104 | -0.074 |
| **400** | -0.751 | -0.711 | -0.672 | -0.632 | -0.592 | -0.553 | -0.513 | -0.473 | -0.434 | -0.394 | -0.354 | -0.315 | -0.275 | -0.235 | -0.196 | -0.156 | -0.116 |
| **500** | -0.956 | -0.906 | -0.857 | -0.807 | -0.757 | -0.708 | -0.658 | -0.609 | -0.559 | -0.509 | -0.460 | -0.410 | -0.361 | -0.311 | -0.261 | -0.212 | -0.162 |
| **600** | -1.164 | -1.104 | -1.045 | -0.985 | -0.925 | -0.866 | -0.806 | -0.747 | -0.687 | -0.628 | -0.568 | -0.509 | -0.449 | -0.390 | -0.330 | -0.271 | -0.211 |
| **700** | -1.374 | -1.304 | -1.235 | -1.166 | -1.096 | -1.027 | -0.957 | -0.888 | -0.818 | -0.749 | -0.679 | -0.610 | -0.541 | -0.471 | -0.402 | -0.332 | -0.263 |
| **800** | -1.587 | -1.507 | -1.428 | -1.348 | -1.269 | -1.190 | -1.110 | -1.031 | -0.952 | -0.872 | -0.793 | -0.713 | -0.634 | -0.555 | -0.475 | -0.396 | -0.317 |
| **900** | -1.801 | -1.712 | -1.623 | -1.533 | -1.444 | -1.355 | -1.265 | -1.176 | -1.087 | -0.998 | -0.908 | -0.819 | -0.730 | -0.640 | -0.551 | -0.462 | -0.373 |
| **1000** | -2.018 | -1.919 | -1.819 | -1.720 | -1.621 | -1.522 | -1.422 | -1.323 | -1.224 | -1.125 | -1.026 | -0.926 | -0.827 | -0.728 | -0.629 | -0.530 | -0.430 |
| **1100** | -2.236 | -2.127 | -2.018 | -1.909 | -1.799 | -1.690 | -1.581 | -1.472 | -1.363 | -1.254 | -1.145 | -1.036 | -0.926 | -0.817 | -0.708 | -0.599 | -0.490 |
| **1200** | -2.456 | -2.337 | -2.218 | -2.099 | -1.980 | -1.860 | -1.741 | -1.622 | -1.503 | -1.384 | -1.265 | -1.146 | -1.027 | -0.908 | -0.789 | -0.670 | -0.551 |
| **1300** | -2.677 | -2.548 | -2.419 | -2.290 | -2.161 | -2.032 | -1.903 | -1.774 | -1.645 | -1.516 | -1.387 | -1.258 | -1.129 | -1.000 | -0.871 | -0.742 | -0.613 |
| **1400** | -2.900 | -2.761 | -2.622 | -2.483 | -2.344 | -2.205 | -2.066 | -1.927 | -1.788 | -1.650 | -1.511 | -1.372 | -1.233 | -1.094 | -0.955 | -0.816 | -0.677 |
| **1500** | -3.123 | -2.975 | -2.826 | -2.677 | -2.528 | -2.379 | -2.231 | -2.082 | -1.933 | -1.784 | -1.635 | -1.486 | -1.338 | -1.189 | -1.040 | -0.891 | -0.742 |
| **1600** | -3.349 | -3.190 | -3.031 | -2.872 | -2.714 | -2.555 | -2.396 | -2.237 | -2.079 | -1.920 | -1.761 | -1.602 | -1.444 | -1.285 | -1.126 | -0.968 | -0.809 |
| **1700** | -3.575 | -3.406 | -3.237 | -3.069 | -2.900 | -2.732 | -2.563 | -2.394 | -2.226 | -2.057 | -1.888 | -1.720 | -1.551 | -1.382 | -1.214 | -1.045 | -0.876 |
| **1800** | -3.802 | -3.624 | -3.445 | -3.266 | -3.088 | -2.909 | -2.731 | -2.552 | -2.373 | -2.195 | -2.016 | -1.838 | -1.659 | -1.481 | -1.302 | -1.123 | -0.945 |
| **1900** | -4.030 | -3.842 | -3.653 | -3.465 | -3.276 | -3.088 | -2.899 | -2.711 | -2.522 | -2.334 | -2.145 | -1.957 | -1.768 | -1.580 | -1.391 | -1.203 | -1.014 |
| **2000** | -4.260 | -4.061 | -3.863 | -3.665 | -3.466 | -3.268 | -3.069 | -2.871 | -2.672 | -2.474 | -2.276 | -2.077 | -1.879 | -1.680 | -1.482 | -1.283 | -1.085 |
| **2100** | -4.490 | -4.282 | -4.073 | -3.865 | -3.657 | -3.448 | -3.240 | -3.032 | -2.823 | -2.615 | -2.407 | -2.198 | -1.990 | -1.782 | -1.573 | -1.365 | -1.157 |
| **2200** | -4.721 | -4.503 | -4.285 | -4.066 | -3.848 | -3.630 | -3.412 | -3.193 | -2.975 | -2.757 | -2.538 | -2.320 | -2.102 | -1.884 | -1.665 | -1.447 | -1.229 |
| **2300** | -4.953 | -4.725 | -4.497 | -4.269 | -4.040 | -3.812 | -3.584 | -3.356 | -3.128 | -2.899 | -2.671 | -2.443 | -2.215 | -1.987 | -1.759 | -1.530 | -1.302 |
| **2400** | -5.186 | -4.948 | -4.710 | -4.472 | -4.234 | -3.995 | -3.757 | -3.519 | -3.281 | -3.043 | -2.805 | -2.567 | -2.329 | -2.091 | -1.852 | -1.614 | -1.376 |
| **2500** | -5.420 | -5.171 | -4.923 | -4.675 | -4.427 | -4.179 | -3.931 | -3.683 | -3.435 | -3.187 | -2.939 | -2.691 | -2.443 | -2.195 | -1.947 | -1.699 | -1.451 |
| **2600** | -5.654 | -5.396 | -5.138 | -4.880 | -4.622 | -4.364 | -4.106 | -3.848 | -3.590 | -3.332 | -3.074 | -2.816 | -2.559 | -2.301 | -2.043 | -1.785 | -1.527 |
| **2700** | -5.889 | -5.621 | -5.353 | -5.085 | -4.818 | -4.550 | -4.282 | -4.014 | -3.746 | -3.478 | -3.210 | -2.942 | -2.675 | -2.407 | -2.139 | -1.871 | -1.603 |
| **2800** | -6.125 | -5.847 | -5.569 | -5.291 | -5.014 | -4.736 | -4.458 | -4.180 | -3.902 | -3.625 | -3.347 | -3.069 | -2.791 | -2.513 | -2.236 | -1.958 | -1.680 |

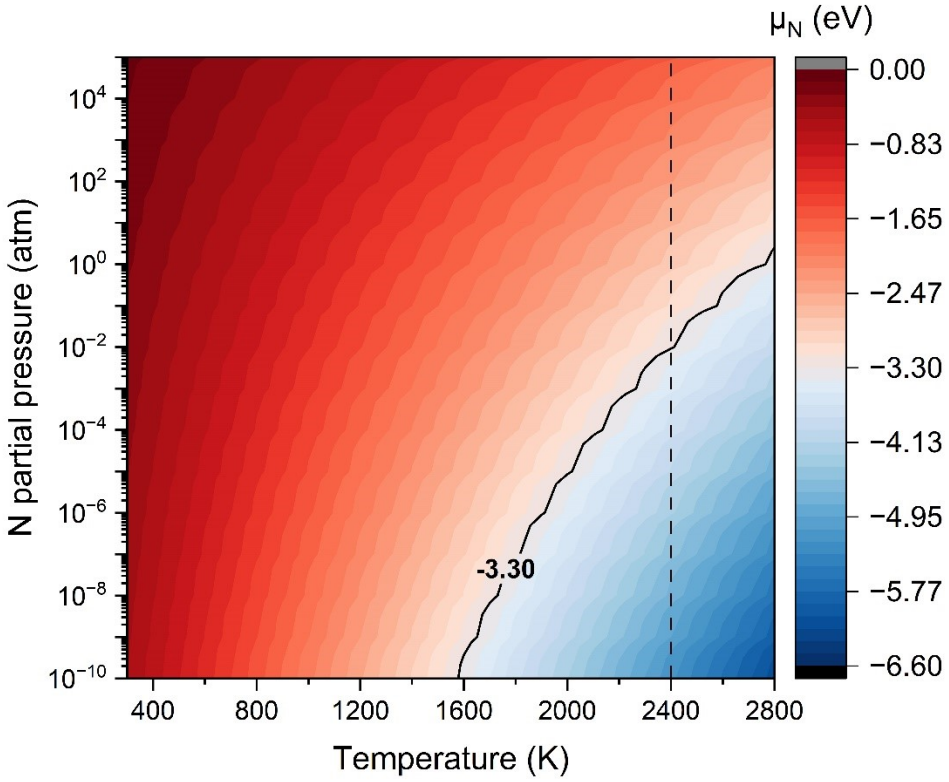


**Figure S4** The nitrogen chemical potential calculated from the experimental thermochemical enthalpy and entropy of $N_2$ from Table S14. The solid line indicates the chemical potential at N-poor limit ($\mu_N =$ -3.296 eV) of AlN formation. The region to the left of the N-poor limit ($\mu_N \geq$ -3.296 eV) represents allowed N partial pressure with respect to temperature.

**Reference for ESI:**


1 I. A. Aleksandrov and K. S. Zhuravlev, *Journal of Physics: Condensed Matter*, 2020, **32**, 435501.

2 L. Zhu, C. R. A. Catlow, Q. Hou, X. Zhang, J. Buckeridge and A. A. Sokol, *J. Mater. Chem. A*, 2023, **11**, 15482–15498.

3 I. Vurgaftman, J. R. Meyer and L. R. Ram-Mohan, *Journal of Applied Physics*, 2001, **89**, 5815–5875.

4 N. S. Kanhe, A. B. Nawale, R. L. Gawade, V. G. Puranik, S. V. Bhoraskar, A. K. Das and V. L. Mathe, *Journal of Crystal Growth*, 2012, **339**, 36–45.

5 Q. Yan, A. Janotti, M. Scheffler and C. G. Van de Walle, *Applied Physics Letters*, 2014, **105**, 111104.

6 B. E. Gaddy, Z. Bryan, I. Bryan, R. Kirste, J. Xie, R. Dalmau, B. Moody, Y. Kumagai, T. Nagashima, Y. Kubota, T. Kinoshita, A. Koukitu, Z. Sitar, R. Collazo and D. L. Irving, *Applied Physics Letters*, 2013, **103**, 161901.

7 Y. Chen, L. Wu, D. Liang, P. Lu, J. Wang, J. Chen, H. Cao and L. Han, *Computational Materials Science*, 2021, **188**, 110169.

8 Y. Zhang, W. Liu and H. Niu, *Physical Review B*, 2008, **77**, 35201.

9 K. Laaksonen, M. G. Ganchenkova and R. M. Nieminen, *Journal of Physics: Condensed Matter*, 2009, **21**, 15803.

10 C. Stampfl and C. G. Van de Walle, *Physical Review B*, 2002, **65**, 155212.

11 Y. Gao, D. Sun, X. Jiang and J. Zhao, *Journal of Applied Physics*, 2019, **125**, 215705.

12 H. Seo, M. Govoni and G. Galli, *Scientific Reports*, 2016, **6**, 20803.

13 P. Boguslawski, E. Briggs, T. A. White, M. G. Wensell and J. Bernholc, *MRS Online Proceedings Library*, 1994, **339**, 693–698.

14 A. Szállás, K. Szász, X. T. Trinh, N. T. Son, E. Janzén and A. Gali, *Journal of Applied Physics*, 2014, **116**, 113702.

15 Z. Xie, Y. Sui, J. Buckeridge, C. R. A. Catlow, T. W. Keal, P. Sherwood, A. Walsh, D. O. Scanlon, S. M. Woodley and A. A. Sokol, *physica status solidi (a)*, 2017, **214**, 1600445.

16 J. Buckeridge, C. R. A. Catlow, M. R. Farrow, A. J. Logsdail, D. O. Scanlon, T. W. Keal, P. Sherwood, S. M. Woodley, A. A. Sokol and A. Walsh, *Phys. Rev. Materials*, 2018, **2**, 54604.

17 K. Kim, W. R. L. Lambrecht, B. Segall and M. van Schilfgaarde, *Physical Review B*, 1997, **56**, 7363–7375.

18 CRC Handbook, *CRC Handbook of Chemistry and Physics*, CRC Press/Taylor & Francis, Boca Raton, FL, USA, 2021.

19 G. Kresse and J. Hafner, *Physical Review B*, 1993, **47**, 558–561.

20 G. Kresse and J. Furthmüller, *Physical Review B*, 1996, **54**, 11169–11186.

21 G. Kresse and D. Joubert, *Phys. Rev. B*, 1999, **59**, 1758–1775.

22 J. P. Perdew, M. Ernzerhof and K. Burke, *The Journal of Chemical Physics*, 1996, **105**, 9982–9985.

23 C. Adamo and V. Barone, *The Journal of Chemical Physics*, 1999, **110**, 6158–6170.